molecular pharmaceutics

Article

Cite This: Mol. Pharmaceutics 2018, 15, 175−185

Cyclic versus Noncyclic Chelating Scaffold for ^{89}Zr-Labeled ZEGFR:2377 Affibody Bioconjugates Targeting Epidermal Growth Factor Receptor Overexpression

Dominik Summer,[†,⊥] Javad Garousi,[‡,⊥] Maryam Oroujeni,[‡,⊥] Bogdan Mitran,[§] Ken G. Andersson,[∥] Anzhelika Vorobyeva,[‡] John Löfblom,[∥] Anna Orlova,[§] Vladimir Tolmachev,[‡] and Clemens Decristoforo*[,†]

[†]Department of Nuclear Medicine, Medical University Innsbruck, Anichstrasse 35, A-6020 Innsbruck, Austria

[‡]Institute of Immunology, Genetic and Pathology, Uppsala University, SE-75185 Uppsala, Sweden

[§]Division of Molecular Imaging, Department of Medicinal Chemistry, Uppsala University, SE-751 83 Uppsala, Sweden

[∥]Division of Protein Technology, KTH Royal Institute of Technology, SE-10691 Stockholm, Sweden

Supporting Information

ABSTRACT: Zirconium-89 is an emerging radionuclide for positron emission tomography (PET) especially for biomolecules with slow pharmacokinetics as due to its longer half-life, in comparison to fluorine-18 and gallium-68, imaging at late time points is feasible. Desferrioxamine B (DFO), a linear bifunctional chelator (BFC) is mostly used for this radionuclide so far but shows limitations regarding stability. Our group recently reported on fusarinine C (FSC) with similar zirconium-89 complexing properties but potentially higher stability related to its cyclic structure. This study was designed to compare FSC and DFO head-to-head as bifunctional chelators for ^{89}Zr-radiolabeled EGFR-targeting ZEGFR:2377 affibody bioconjugates. FSC-ZEGFR:2377 and DFO-ZEGFR:2377 were evaluated regarding radiolabeling, *in vitro* stability, specificity, cell uptake, receptor affinity, biodistribution, and microPET-CT imaging. Both conjugates were efficiently labeled with zirconium-89 at room temperature but radiochemical yields increased substantially at elevated temperature, 85 °C. Both ^{89}Zr-FSC-ZEGFR:2377 and ^{89}Zr-DFO-ZEGFR:2377 revealed remarkable specificity, affinity and slow cell-line dependent internalization. Radiolabeling at 85 °C showed comparable results in A431 tumor xenografted mice with minor differences regarding blood clearance, tumor and liver uptake. In comparison ^{89}Zr-DFO-ZEGFR:2377, radiolabeled at room temperature, showed a significant difference regarding tumor-to-organ ratios. MicroPET-CT imaging studies of ^{89}Zr-FSC-ZEGFR:2377 as well as ^{89}Zr-DFO-ZEGFR:2377 confirmed these findings. In summary we were able to show that FSC is a suitable alternative to DFO for radiolabeling of biomolecules with zirconium-89. Furthermore, our findings indicate that ^{89}Zr-radiolabeling of DFO conjugates at higher temperature reduces off-chelate binding leading to significantly improved tumor-to-organ ratios and therefore enhancing image contrast.

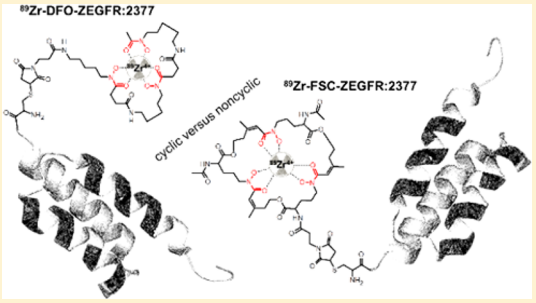

KEYWORDS: *FSC, DFO, zirconium-89, EGFR, affibody, PET*

INTRODUCTION

The positron-emitting radiometal zirconium-89 has attracted great attention for targeted molecular imaging due to its long half-life of 78.4 h enabling high-resolution positron emission tomography (PET) imaging at late time points. This is of particular interest for radiolabeling of biomolecules undergoing slow distribution *in vivo*. Investigations on the coordination chemistry of $^{89}Zr^{4+}$ in aqueous media indicate the preference of an octadentate ligand for stable complexation of the radionuclide.[1,2] Despite intensive work on the design of novel octadentate chelators for zirconium-89,[3−9] the linear siderophore-based hexadentate ligand desferrioxamine B (DFO) still is the most widely used chelator for ^{89}Zr-radiopharmaceuticals under clinical investigation, in particular monoclonal antibodies.[10−12] This is despite the fact that the unsaturated coordination of zirconium-89 is reported to be associated with release of radionuclide leading to increased radiation burden for patients due to the osteophilicity of the free ^{89}Zr-cation.[13,14] Our group recently reported on the application of fusarinine C (FSC), a siderophore-based chelator derived from *Aspergillus fumigatus*.[15] FSC has comparable complexing properties toward zirconium-89 to DFO but potentially improved stability due to the cyclic structure of the molecule.[16] Even if that study has proven FSC to be an interesting alternative to DFO for radiolabeling with zirconium-89, the results obtained from a

Received: September 11, 2017
Revised: November 6, 2017
Accepted: November 21, 2017
Published: November 21, 2017

DOI: 10.1021/acs.molpharmaceut.7b00787
Mol. Pharmaceutics 2018, 15, 175−185

peptide-based setting are not entirely translatable for the evaluation of larger biomolecules. Imaging probes based on nonimmunoglobulin engineered scaffold proteins (ESP) represent a higher level of complexity comparted to radiolabeled short peptides.[17,18] Unlike peptides, ESP possess tertiary structure. Although ESP usually refold after denaturing (e.g., under harsh radiolabeling conditions), chelators or other pendant group might interfere with refolding resulting in appreciable loss of binding capacity.[19,20] An intricate spatial structure of ESP and larger size (molecular weight of 4 to16 kDa) might lead to formation of "chelator pockets" of electron donating side-chains, which compete for binding of a radiometal with a bifunctional chelators.[21,22] Although ESP-based probes can often provide good imaging a few hours after injection, in some cases one or several days are required to reach an appropriate contrast.[23,24] A long-lived positron-emitting label would be attractive for such ESP. Therefore, a head-to-head comparison of FSC and DFO (structures are presented in Figure 1) conjugated to an affibody molecule targeting epidermal growth factor receptor (EGFR) was initiated.

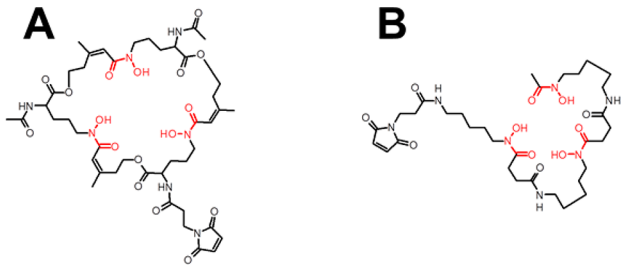

Figure 1. Structures of maleimide-derivatized FSC (A) and DFO (B).

EGFR is a transmembrane tyrosine kinase (TK) and as a promoter for cell proliferation involved in various malignancies like nonsmall-cell lung cancer (NSCLC), head and neck squamous cell carcinoma (HNSCC), colorectal cancer, glioblastoma, pancreatic, and breast cancer.[25] Detection of EGFR overexpression enables to stratify patients with NSCLC and HNSCC for an adequate therapy[26−30] and blocking of EGFR signaling by monoclonal antibodies (e.g., cetuximab, panitumumab) or specific tyrosine kinase inhibitors (e.g., gefitinib) improves survival of patients with EGFR-over-expressing cancers.[31] However, a highly complex signaling pathway of EGFR, the susceptibility for different mutations leading to EGFR overexpression and the discrepancy in primary and metastatic stage of disease[32] due to clonal selection makes it a challenging target for therapeutic decisions. In contrast to immunohistochemistry (IHC), which is currently used for patient stratification (determination of EGFR expression), repeatable and noninvasive targeted PET-imaging provides a highly attractive alternative for fundamental decisions regarding first-line treatment and therapy management. It has to be noted that an appreciable expression of EGFR in normal hepatocytes is a challenge for its radionuclide molecular imaging due to sequestering of an imaging agent from blood. However, this problem might be solved by accurate adjustment of injected tracer mass.[33]

Velikyan and co-workers[34] reported on a highly affine and specifically binding PET-imaging agent, DOTA-hEGF, radiolabeled with gallium-68 for visualization of EGFR over-expression, but the short half-life of gallium-68 and especially the strong agonistic effect of the endogenous ligand limits this application. In contrast mAbs show absence of agonistic effects and imaging of EGFR associated malignancies with radiolabeled antibodies is generally possible but low tumor-to-organ ratios due to enhanced circulation time in the blood pool (up to days) remains disadvantageous regarding imaging contrast.[35−37] Contrary to this, affibody molecules represent a rather new class of small (7 kDa), high affinity binders derived from B-domain of protein A[38] with potential improved pharmacokinetics compared to mAbs. They have proven their value in a number of preclinical studies as EGFR targeting agents.[39−42] Importantly, the ZEGFR:2377 affibody molecule has an equal affinity to human and murine EGFR, which helps to address the issue of a tracer interaction with EGFR expressed in normal tissues.[43] Previous studies have demonstrated that radiolabeled ZEGFR:2377 is slowly internalized after binding to EGFR-expressing cells, and the majority of the tracers is therefore remaining on the cell surface.[43] Due to this reversible binding, the normal EGFR-expressing tissues act as depot releasing dissociated radiolabeled ZEGFR:2377 back to bloodstream. This results in relatively slow clearance from blood and therefore an optimal imaging time for this affibody molecule is 24 h after injection.[40−42,44] The use of PET offers advantages of better resolution and smaller influence of partial volume effect in imaging of small metastases. For the moment, zirconium-89 is only positron emitter with sufficiently long half-life, which is commercially available worldwide. The goal of this study was to compare the use of cyclic versus noncyclic chelators for radiolabeling of the anti-EGFR binding affibody ZEGFR:2377 with zirconium-89 for imaging EGFR overexpression.

EXPERIMENTAL SECTION

Analytical RP-HPLC. Reversed-phase high-performance liquid chromatography analysis was carried out on an UltiMate 3000 RS UHPLC pump, UltiMate 3000 autosampler, Ultimate 3000 column compartment (25 °C oven temperature), UltiMate 3000 Variable Wavelength Detector (Dionex, Germering, Germany) using acetonitrile (ACN)/H_2O/0.1% trifluoroacetic acid (TFA) as mobile phase with varied settings.

A. ACE 3 μm C_{18} 100 Å 150 × 3.0 mm (ACE, Aberdeen, Scotland) column; flow rate of 0.6 mL/min; UV detection at λ = 220 nm; gradient: 0.0−1.0 min 10% ACN, 1.0−10.0 min 10−30% ACN, 10.0−11.0 min 30−60% ACN, 11.0−13.0 min 60% ACN, 13.0−17.0 60−10% ACN.

B. Jupiter 4 μm Proteo 90 Å 250 × 4.6 mm (Phenomenex Ltd. Aschaffenburg, Germany) column; flow rate of 1 mL/min; UV detection at λ = 220 nm; gradient: 0.0−3.0 min 0% ACN, 3.0−23.0 min 0−80% ACN, 23.0−25.0 min 80% ACN, 25.0−30.0 min 0% ACN.

C. Jupiter 5 μm C_{18} 300 Å 150 × 4.6 mm (Phenomenex Ltd. Aschaffenburg, Germany) column; flow rate of 2 mL/min; UV detection at λ = 280 nm; gradient: 0.0−1.0 min 30% ACN, 1.0−15.0 min 30−60% ACN, 15.0−17.0 min 60% ACN, 17.0−20.0 min 60−30% ACN.

Preparative RP-HPLC. Sample purification via RP-HPLC was performed on a Gilson 322 Pump with a Gilson UV/vis-155 detector and the single fractions were collected by a PrepFC automatic fraction collector (Gilson, Middleton, WI, USA). UV detection at λ = 220 nm and a flow rate of 2 mL/min on a Eurosil Bioselect Vertex Plus 30 × 8 mm 5 μm C_{18}A 300 Å precolumn and Eurosil Bioselect Vertex Plus 300 × 8 mm 5 μm C_{18}A 300 Å column (Knauer, Berlin, Germany) were

DOI: 10.1021/acs.molpharmaceut.7b00787
Mol. Pharmaceutics 2018, 15, 175−185

applied using following ACN/H_2O/0.1% TFA multistep gradients.

Gradient A. 0.0−1.0 min 0% ACN, 1.0−20.0 min 0−50% ACN, 20.0−23.0 min 50% ACN, 23.0−25.0 min 0% ACN

Gradient B. 0.0−1.0 min 20% ACN, 1.0−25.0 min 20−60% ACN, 25.0−30.0 min 60% ACN, 30.0−35.0 min 20 % ACN

Gradient C. 0.0−1.0 min 20% ACN, 1.0−45.0 min 20−80% ACN, 45.0−50.0 min 100% ACN, 50.0−55.0 min 20 % ACN

MALDI-TOF MS. Matrix-assisted laser desorption/ionization time-of-flight mass spectrometry was performed on a Bruker microflex benchtop MALDI-TOF MS (Bruker Daltonics, Bremen, Germany). Samples were prepared on a micro scout target (MSP96 target ground steel BC, Bruker Daltonics) via dried-droplet method using α-cyano-4-hydroxy-cinnamic acid (HCCA, Sigma-Aldrich, Handels GmbH, Vienna, Austria) as matrix. All spectra were recorded by summarizing 800 laser shots per spot and Flex Analysis 2.4 software was used for data processing.

ESI-MS. Samples were purified by ZipTip C18 pipet tips (Millipore) according to the manufacturer's instructions prior to nanoLC-ESI-MS analysis. Purified samples were analyzed using an UltiMate 3000 nano-HPLC system coupled to a Q Exactive HF mass spectrometer (both Thermo Scientific, Bremen, Germany) equipped with a Nanospray Flex ionization source. The samples were separated on a homemade fritless fused-silica microcapillary column (75 μm i.d. × 280 μm o.d. × 10 cm length) packed with 3 μm reversed-phase C18 material (Reprosil). Solvents for HPLC were 0.1% formic acid (solvent A) and 0.1% formic acid in 85% acetonitrile (solvent B). The gradient profile was as follows: 0−2 min, 4% B; 2−40 min, 4−50% B; 40−45 min, 50−100% B, and 45−50 min, 100% B. The flow rate was 250 nL/min. The Q Exacitve HF mass spectrometer was operating in the data dependent mode selecting the top 20 most abundant isotope patterns with charge >1 from the survey scan with an isolation window of 1.6 mass-to-charge ratio (m/z). Survey full scan MS spectra were acquired from 300 to 1750 m/z at a resolution of 60,000 with a maximum injection time (IT) of 120 ms, and automatic gain control (AGC) target 1e6. The selected isotope patterns were fragmented by higher-energy collisional dissociation (HCD) with normalized collision energy of 28 at a resolution of 30,000 with a maximum IT of 120 ms, and AGC target 5e5.

Precursor Preparation. *[Fe]Fusarinine C ([Fe]FSC).* Fusarinine C (FSC) could be obtained from fungal culture in good yield as previously described.[45] Briefly, the iron saturated culture media was passed through a C18 cartridge and the [Fe]FSC was eluted with methanol to give a red brown colored solid after evaporating the organic solvent. A sufficient purity (>90%) permitted its use for further derivatization without additional purification. Analytical data: RP-HPLC (setting A) t_R = 6.3 min; MALDI TOF-MS: m/z [M+H]+ = 780.86 [$C_{33}H_{51}FeN_6O_{12}$; exact mass: 779.63 (calculated)].

N,N′-Diacetyl-[Fe]Fusarinine C (dAc[Fe]FSC). An aliquot of 500 μL [Fe]FSC (32 mM) was dissolved in MetOH/DMF (9:1) and reacted with 5 μL of acetic anhydride (7.5 mg, 0.07 mmol) for 5 min at room temperature (RT) under vigorously stirring. After analytical RP-HPLC analysis (setting A), the resulting mixture of mono- (t_R = 7.7 min), di- (t_R = 9.3 min), and triacetylfusarinine C (t_R = 10.7 min) in a ratio of 1:2:1 was immediately purified via preparative RP-HPLC using gradient A (t_R = 19.4 min) to obtain dAc[Fe]FSC in high purity (>95%). MALDI TOF-MS: m/z [M+H]+ = 864.68 [$C_{37}H_{55}FeN_6O_{14}$; exact mass: 863.709 (calculated)].

N,N′-Diacetyl-N″-(3-maleinimidopropionyl) Fusarinine C (dAcFSC-mal). dAc[Fe]FSC (10 mg, 11.6 μmol) was dissolved in 1 mL anhydrous dimethylformamide ($DMF_{anh.}$). After adding 1.1 equiv (3.4 mg) of 3-(maleimido)propionic acid *N*-hydroxysuccinimide ester (Sigma-Aldrich, Handels GmbH, Vienna, Austria) in 200 μL dry DMF and 5 μL of Huenig's base (*N,N*-diisopropylethylamine, DIPEA), the mixture was stirred for 2 h at ambient temperature. When completion of the reaction was confirmed by analytical RP-HPLC (setting A; t_R = 11.8 min) the organic solvent was evaporated. Hereafter 2 mL of disodium EDTA (100 mM) were added and stirring was continued overnight for iron removal (setting A; t_R = 12.6 min). Finally the product was isolated via preparative RP-HPLC (gradient B; t_R = 19.9 min) and freeze-dried to give a colorless solid (9.9 μmol, 85% of theoretical yield, purity of >96%, MALDI TOF-MS: m/z [M+H]+ = 963.25, [$C_{44}H_{63}N_7O_{17}$; exact mass: 962.01 (calculated)].

Preparation of EGFR-Targeting Bioconjugates. Single C-terminal cysteine bearing affibody molecule (anti-EGFR ZEGFR:2377) was produced as previously described[43] and was conjugated to three-hydroxamate bifunctional chelators via maleimide-sulfhydryl cross-link reaction to facilitate radiolabeling with zirconium-89. Conjugation of acyclic deferoxamine (DFO) to provide DFO-ZEGFR:2377 was conducted according to Garousi and co-workers.[42] Coupling of cyclic fusarinine C derivative (dAc-FSC-mal) was carried out as follows. The disulfide bond stabilized anti-EGFR ZEGFR:2377-dimer (ESI-MS 14780.25 Da) was dissolved in phosphate buffered saline (PBS, pH 7.4) to a concentration of 1 mg/mL and after adding a 10-fold molar excess of tris(2-carboxyethyl)-phosphine hydrochloride (TCEP, Sigma-Aldrich, Handels GmbH, Vienna, Austria), freshly prepared in 100 μL PBS, the mixture was incubated at 37 °C to reduce intermolecular disulfide bonds. After 1 h incubation time, reduction completion was confirmed by ESI-MS (7390.68 Da) and reduced affibody molecules were purified via size exclusion chromatography by using disposable, PBS/BSA (0.1%) pre-equilibrated PD-10 column (GE Healthcare, Vienna, Austria) according to manufacturer's protocol. Hereafter 20-fold molar excess of dAcFSC-mal was dissolved in PBS and added to anti-EGFR ZEGFR:2377 containing fraction. After 2 h reaction time at RT, when ESI-MS showed complete consumption of unconjugated affibody molecule the bioconjugate (further designated as FSC-ZEGFR:2377) was isolated by preparative RP-HPLC (gradient C; t_R = 27.2 min) and was obtained as colorless solid after lyophilization (0.18 μmol; 66.4% of theoretical yield). Purity of the bioconjugate (>96%) was confirmed by analytical RP-HPLC (setting B: t_R = 17.01 min and setting C: t_R = 7.99 min) and ESI-MS analysis to confirm the identity was in good agreement with the expected value (ESI-MS 8352.12 Da measured; 8352 Da calculated).

Radiolabeling with Zirconium-89. ^{89}Zr-oxalic acid solution (1M) was purchased from PerkinElmer (Waltham, US). ZEGFR:2377 targeting bioconjugates were labeled with zirconium-89 according to following protocol, corresponding to a modified variant of Vosjan and co-workers.[46] ^{89}Zr solution (8.7 μL, 10−12 MBq) was neutralized by adding 8.3 μL of Na_2CO_3 (1M) and incubated for 3 min at RT. Hereafter, 66.7 μL of HEPES buffer (0.5M; pH 6.98) was added to the radionuclide containing solution. After subsequent addition of 20 μL of bioconjugate solution (1 μg/μL in H_2O/EtOH 90/10 v/v), the resulting mixture was incubated up to 120 min at 28 and 85 °C, respectively. Radiolabeling was monitored by radio

DOI: 10.1021/acs.molpharmaceut.7b00787
Mol. Pharmaceutics 2018, 15, 175−185

instant thin layer chromatography (*radio*-ITLC) using silica gel-impregnated glass microfiber sheets (ITLC-SG strips, Varian, Lake Forest, CA) as stationary and 0.2 M citric acid (pH 5) as mobile phase. Distribution of the radioactivity among the strips was measured on Cyclone Phosphor Storage Screen using OptiQuant software for data processing (both Packard Instrument Company, Meriden, CT, US) as well as Fujifilm Bioimaging Analyzers (BAS) 1800II using MultiGauge V3.0 analysis software (both Fujifilm, Tokyo, Japan). Radiolabeled bioconjugates were purified for further studies using phosphate buffer saline pre-equilibrated NAP-5 size exclusion columns (GE Healthcare, Uppsala, Sweden) according to manufacturer's protocol.

EDTA-Challenging Assessment. Aliquots of 50 μL of zirconium-89 labeled NAP-5 purified tracers (1.8 nmol) were incubated in duplicates with 1000-fold excess of ethylenediaminetetraacetic acid (EDTA) and in PBS as a control. Transchelation ability was evaluated at 1, 2, and 24 h via *radio*-ITLC measurement as described above, where radiolabeled conjugate remains at the start while ^{89}Zr-EDTA migrates with the solvent front.

SDS-PAGE. Sodium dodecyl sulfate polyacrylamide gel electrophoresis was carried out on XCell SureLock system at 200 V constant for 30 min using NuPAGE 12% Bis-Tris Gel, LDS sample and MES running buffer (Invitrogen AB Foster City, CA, USA).

In Vitro Studies. High level EGFR-expressing A431 human epidermoid carcinoma and MDA468 human breast cancer as well as low level EGFR-expressing DU-145 human prostate cancer cell lines were purchased from American Type Culture Collection (ATCC, via LGC Promochem, Borås, Sweden). Cells were grown in a humidified atmosphere of 95% air/5% carbon dioxide using RPMI-1640 media supplemented with 10% v/v fetal bovine serum (FBS) and 1% v/v Penicillin-Streptomycin-Glutamin (PSG) solution (= complete media).

For binding specificity studies, cells were seeded in 6-well plates (4×10^5 cells/dish for A431 and MDA-468; 1×10^6 cells/dish for DU-145) 3 days before the experiment. On the day of the experiment media was aspirated and all dishes were washed with 2 mL of RPMI-1640 media without additives (= incomplete media). Three sets of dishes were blocked by adding 1 mL complete media containing 0.5 μM blocking agent (cetuximab, His_6-ZEGFR:2377 affibody molecule or bevacizumab in 100-fold molar excess over radioligand) while three dishes remained unblocked containing 1 mL complete media and the plate was left for 15 min at RT. Hereafter 1 mL of the radioligand solution (5 nM; $\sim 4 \times 10^5$ cpm) was added to all dishes and cells were incubated at 37 °C. Incubation media was removed after 1h followed by a washing step with 2 mL of incomplete media. After addition of 500 μL trypsin solution to each well the plate was kept for 30 min at 37 °C to detach the cells. The cell suspension was diluted to 1 mL by adding 500 μL of incomplete media and after extensive resuspension an aliquot of 10 μL was taken to determine the number of cells/mL via automated cell counter (TC20, Bio-Rad, Sweden) while the rest of each dish was collected in a plastic vial. All dishes were washed with 1 mL incomplete media, the supernatant was added to the plastic vial and samples were measured using an automated gamma-counter (Wizard 3″, PerkinElmer, Waltham, MA, USA).

For cellular processing dishes were seeded with A431 and MDA468 cells in a density of 8×10^5 per dish and left to grow overnight. Hereafter, cells were washed with 1 mL incomplete media and 1 mL complete media was added. Finally cells were incubated with 1 mL radioligand solution (5 nM in complete media) at 37 °C for 1, 2, 4, 8, and 24 h in triplicates. At the appointed time, the incubation media was aspirated from the dishes, cells were washed with 2 mL ice-cold incomplete media and the supernatant was discarded. To determine the membrane-bound amount of radiolabeled conjugate cells were treated at RT as follows. First cells were incubated for 15 min with 1 mL acid wash buffer (0.1 M glycine buffer, pH 2.5, containing 4 M urea solution) and after collecting the supernatant this step was repeated with 1 min incubation and acid wash fractions were pooled. After this, cells were rinsed twice with 1.5 mL PBS buffer combining the fractions. Subsequently after PBS buffer collection 1.5 mL of phosphate buffer (pH 8.0) was added to each dish and cells were incubated for 15 min. Phosphate buffer was collected followed by a second basic wash step and phosphate buffer fractions were pooled. To determine the internalized amount of radioligand cells were lysed by adding 1 mL of sodium hydroxide solution (1 M NaOH) and dishes were incubated at 37 °C for at least 45 min. NaOH fractions were collected and the step was repeated without incubation but using a cell scraper. Alkaline fractions were pooled and all fractions were taken for gamma-counter measurement.

Real-time receptor interaction measurements were carried out on LigandTracer Yellow instrument (Ridgeview Instruments AB, Vänge, Sweden) according to previous published protocol.[47] Briefly, living A431 cells were incubated with increasing concentrations (0.33, 1, and 3 nM) of zirconium-89 labeled EGFR-targeting bioconjugates to determine binding kinetics. After replacement of incubation media by fresh cell culture media the dissociation rate was monitored and the obtained data were analyzed using InteractionMap software (Ridgeview Diagnostics AB, Uppsala, Sweden) to calculate receptor affinity.

In Vivo Studies. Biodistribution and imaging studies in tumor xenograft bearing female outbred BALB/c nu/nu mice (Taconic M&B a/S, Ry, Denmark) were conducted under xylazine/ketamine anesthesia to minimize animal suffering and number of animals was reduced as much as possible, this being in accordance with Swedish national regulation on laboratory animals' protection and approval by the Ethics Committee for Animal Research in Uppsala (permission C 4/2016). For tumor xenograft preparation, 1×10^7 A431 cells were injected subcutaneously to the right hind leg and the tumors were grown for 2 weeks. For biodistribution experiments mice were randomized into five groups with four mice. Only one group was pretreated by subcutaneous injection of 10 mg cetuximab per mouse 24 h before the experiment to determine *in vivo* specificity of ^{89}Zr-FSC-ZEGFR:2377 as specificity of ^{89}Zr-DFO-ZEGFR:2377 has been shown before.[42] Zirconium-89 labeled bioconjugates were injected to mice via tail vain (40 kBq in 100 μL PBS per mouse) and the tracer dose was adjusted to 38 μg per mouse with nonlabeled bioconjugate. Distribution of radioactivity among blood and organs was measured 3 and 24 h post injection (p.i).

Whole body positron emission tomography (PET)/computed tomography (CT) imaging was performed using Triumph trimodality system (TriFoil Imaging, Inc., Northridge, CA, USA) at 3 and 24 h p.i. The animals (n = 2 per time point) were injected with 4 MBq of zirconium-89 labeled bioconjugate (dose adjustment with nonlabeled tracer to 38 μg per mouse) and sacrificed by CO_2 asphyxiation immediately before being

DOI: 10.1021/acs.molpharmaceut.7b00787
Mol. Pharmaceutics 2018, 15, 175−185

Table 1. Radiolabeling of FSC-ZEGFR:2377 and DFO-ZEGFR:2377 with Zirconium-89 (2.4 nmol, pH 7 at 28 °C and 85°C)[a]

	radiochemical yield (RCY %)			
	FSC-ZEGFR:2377		DFO-ZEGFR:2377	
time [min]	28 °C	85 °C	28 °C	85 °C
10	33.7 ± 10.9	83.6 ± 7.9**	37.9 ± 20.6	96.5 ± 3.0*
30	63.2 ± 11.6	96.8 ± 1.8**	50.2 ± 16.3	97.5 ± 1.4*
45	n.d	n.d	62.3 ± 14.4	98.2 ± 1.0*
60	82.7 ± 10.3	97.7 ± 0.1	74.4 ± 9.9	98.5 ± 0.6*
90	88.1 ± 7.4	98.6 ± 1.0	81.8 ± 0.2	n.d
120	91.9 ± 5.8	n.d	83.1 ± 2.6	n.d

[a]Data were calculated from ITLC measurement of the nonpurified bioconjugates and are presented as mean ± standard deviation (n = 4), statistical analysis was performed using the Student's t test with P values indicating very significant (** $P < 0.01$) and significant (* $P < 0.05$) difference between various temperature.

Table 2. Stability of ^{89}Zr-FSC-ZEGFR:2377 and ^{89}Zr-DFO-ZEGFR:2377 in PBS and EDTA[a]

	^{89}Zr-FSC-ZEGFR:2377				^{89}Zr-DFO-ZEGFR:2377			
	28 °C		85 °C		28 °C		85 °C	
time [h]	PBS	EDTA	PBS	EDTA	PBS	EDTA	PBS	EDTA
1	96.8 ± 0.1	94.6 ± 0.3	99.9 ± 0.1	98.9 ± 0.2	99.3 ± 0.2	95.9 ± 0.7	96.9 ± 0.6	94.3 ± 0.3
2	96.5 ± 0.5	93.5 ± 0.5	99.9 ± 0.1	99.0 ± 0.2	90.7 ± 4.5	81.7 ± 1.5	89.8 ± 1.3	84.2 ± 1.5
24	90.2 ± 0.1	85.7 ± 0.4	98.8 ± 0.3	97.6 ± 0.3	88.3 ± 1.3	67.7 ± 3.6	85.8 ± 0.4	63.3 ± 0.1

[a]Data were calculated from ITLC measurement and are presented as average ± maximum error (n = 2).

placed in the camera. The CT scans were performed at the following parameters: 80 mm field of view (FOV); 1.48 magnification; one frame and 512 projections for 2.13 min followed by PET scans conducted for 1 h. CT raw files were reconstructed by filter back projection (FBP). PET data were reconstructed using OSEM-3D (20 iterations). CT data were used for scatter and attenuation correction. PET and CT files were fused and analyzed using PMOD v3.510 (PMOD Technologies Ltd., Zurich, Switzerland). Coronal and sagittal PET-CT images are presented as maximum intensity projections (MIP) in RGB color scale.

Autoradiography. After the gamma-counter measurement was completed, tumors were frozen at −80 °C and embedded in a cryomedium. Frozen tumors were cut in serial sections (20 μm thick) using a cryomicrotome and thaw-mounted on glass slides. For the digital autoradiography, the slides with sections were put in an X-ray cassette and exposed to phosphor screens overnight. The screens were scanned on a Cyclone Storage Phosphor System at a resolution of 600 dpi and analyzed using the OptiQuant software (PerkinElmer, USA).

After that, the same tumor sections were stained using hematoxylin and eosin following a standard protocol. Digital scanning of hematoxylin and eosin stained sections at 5× magnification was performed at the SciLifeLab Tissue Profiling Facility, Uppsala University. Digital images were analyzed using Aperio ImageScope software (Leica Biosystems, USA).

Statistical Analysis. In order to determine statistical differences, two-tailed t test was performed using GraphPad Prism (version 4.00 for Windows GraphPad Software).

RESULTS

Precursor Synthesis. Preparation of EGFR targeting bioconjugates was straightforward utilizing maleimide-sulfhydryl cross-link reaction for chelator-affibody conjugation. DFO-ZEGFR:2377 and FSC-ZEGFR:2377, respectively, were obtained in good yield and high chemical purity (>95%) and ESI-MS analysis was in excellent agreement with theoretical calculations (see Supporting Information).

^{89}Zr Radiolabeling and Stability. Radiolabeling of FSC-ZEGFR:2377 as well as DFO-ZEGFR:2377 with zirconium-89 in HEPES buffer at neutral pH was performed according to the protocol of Vosjan and co-workers[46] with slight variations regarding temperature (Table 1). Both bioconjugates showed slow complex formation over a period of 2 h at 28 °C while the labeling rate could be increased significantly when the reaction was carried out at 85 °C. The radiochemical yield (RCY) was already >96% after 30 min when elevated temperature was used whereas the corresponding RCY was around 60% for ^{89}Zr-FSC-ZEGFR:2377 and around 50% for ^{89}Zr-DFO-ZEGFR:2377 at 28 °C. After quantitative radiolabeling (RCY > 90%), ^{89}Zr-FSC-ZEGFR:2377 and ^{89}Zr-DFO-ZEGFR:2377 were purified via disposable NAP-5 columns with a recovery rate ranging from 70 to 85% and a radiochemical purity of >99%. Radio-SDS-PAGE analysis confirmed the purity the isolated bioconjugates. Stability assessment of ^{89}Zr-labeled conjugates is summarized in Table 2. ^{89}Zr-FSC-ZEGFR:2377 labeled at 28 °C showed release of zirconium-89 in PBS (10%) and EDTA (15%) after 24 h while radiolabeling at elevated temperature increased the complex stability in both media (>97%). Corresponding studies with ^{89}Zr-DFO-ZEGFR:2377 showed ^{89}Zr-release of ∼10% in PBS and ∼30% in EDTA without major difference regarding radiolabeling temperature. As radiolabeling at higher temperature was more efficient this condition was preferred for further experiments, *in vitro* and *in vivo* characterization, respectively.

***In Vitro* Characterization.** Real-time LigandTracer EGFR affinity measurement on living A431 cells is presented in Figure 2. Both, ^{89}Zr-FSC-ZEGFR:2377 and ^{89}Zr-DFO-ZEGFR:2377, showed rapid EGFR association (k_a) and slow dissociation (k_d) rate from the receptor. This results in a very high and comparable receptor affinity for both ^{89}Zr-FSC-ZEGFR:2377 (56 ± 8 pM) and ^{89}Zr-DFO-ZEGFR:2377 (104 ± 54 pM).

DOI: 10.1021/acs.molpharmaceut.7b00787
Mol. Pharmaceutics 2018, 15, 175−185

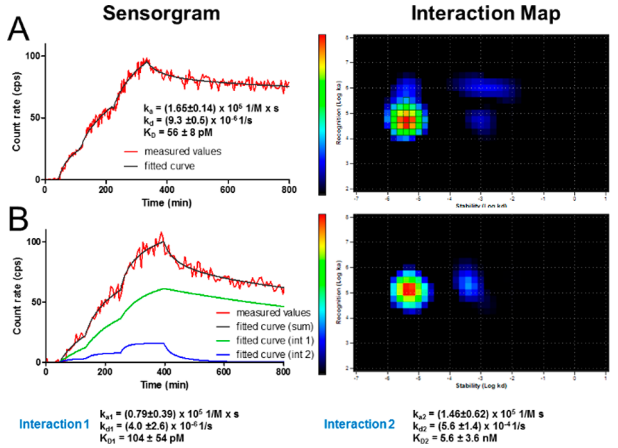

Figure 2. LigandTracer sensorgram and InteractionMap of ^{89}Zr-FSC-ZEGFR:2377 (A) and ^{89}Zr-DFO-ZEGFR:2377 (B) binding to EGFR-expressing A431 cells. Binding was measured at three different concentrations (0.33, 1, and 3 nM).

Receptor specificity for both conjugates is summarized in Figure 3. ^{89}Zr-FSC-ZEGFR:2377 showed 18.7 ± 0.9% (A431)

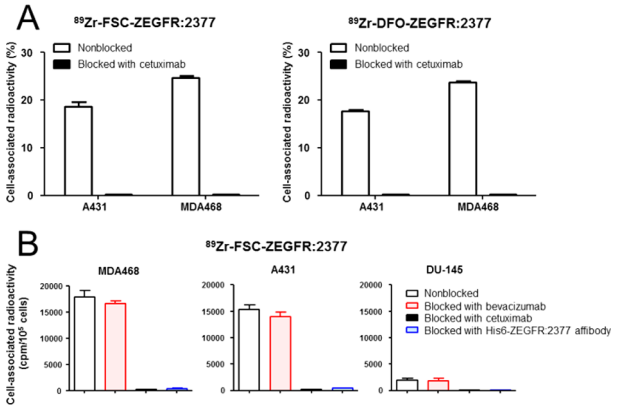

Figure 3. (A) Receptor specificity studies on A431 and MDA468 cells for ^{89}Zr-FSC-ZEGFR:2377 and ^{89}Zr-DFO-ZEGFR:2377 [data expressed as % of total added activity; mean ± SD; n = 3]; (B) extended specificity study for ^{89}Zr-FSC-ZEGFR:2377 on cells with different level of EGFR-expression [data presented as counts per minute (CPM) per 10^5 cells, mean ± SD; n = 3]. Error bars might not be seen because they are smaller than the symbols.

and 24.7 ± 0.4% (MDA468) of total added activity bound to the cells after 1 h-incubation. Corresponding studies with ^{89}Zr-DFO-ZEGFR:2377 resulted in 17.7 ± 0.3% (A431) and 23.8 ± 0.2% (MDA468) cell-associated radioactivity. Pretreatment of A431 and MDA468 cells with EGFR specific antibody cetuximab led to a highly significant (<0.3% of total activity; $P < 1 \times 10^{-6}$) reduction of binding of ^{89}Zr-labeled affibody bioconjugates indicating highly specific targeting properties (Figure 3A). Furthermore, extended specificity studies (Figure 3B) with ^{89}Zr-FSC-ZEGFR:2377 showed level of EGFR-expression dependent cell binding. Receptor saturation with cetuximab and ZEGFR:2377 affibody molecule (His_6-ZEGFR:2377) resulted again in highly significant reduction ($P < 2 \times 10^{-4}$) of ^{89}Zr-FSC-ZEGFR:2377 binding to the cells while blocking studies with bevacizumab showed no significant reduction, as this antibody is vascular endothelial growth factor (VEGF) and not EGFR specific, substantiating the highly specific EGFR mediated cell binding of FSC-ZEGFR:2377 biomolecule. Cellular processing profile of ^{89}Zr-FSC-ZEGFR:2377 and ^{89}Zr-DFO-ZEGFR:2377 by MDA468 and A431 cells is presented in Figure 4. Both bioconjugates showed

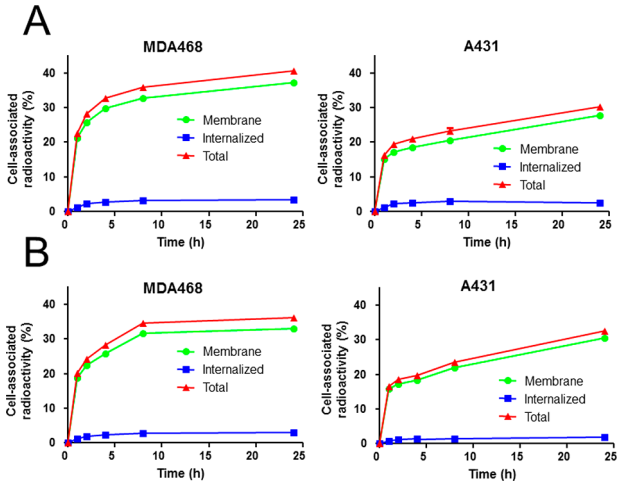

Figure 4. Cellular processing of ^{89}Zr-FSC-ZEGFR:2377 (A) and ^{89}Zr-DFO-ZEGFR:2377 (B) by continuous incubation on A431 and MDA468 cells (mean ± SD; n = 3). Data are presented as percentage of total radioactivity and error bars might not be seen because they are smaller than the symbols.

very similar internalization, which was cell-line dependent and relatively slow as the uptake of cell-bound radioactivity was ~6% in A431 and ~9% in MDA468 cells after 24 h-incubation.

***In Vivo* Characterization.** Specificity of ^{89}Zr-FSC-ZEGFR:2377 in tumor xenografted mice is presented in Figure 5 while *in vivo* specificity of ^{89}Zr-DFO-ZEGFR:2377 has

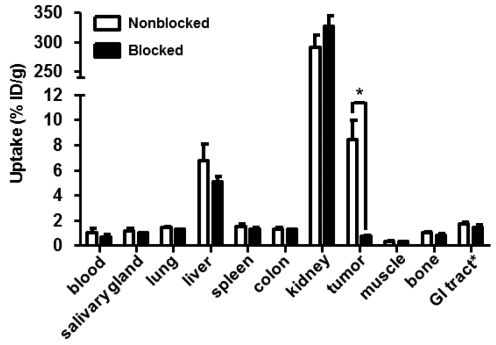

Figure 5. Specificity of ^{89}Zr-FSC-ZEGFR:2377 in A431 tumor xenograft bearing BALB/C nu/nu 3 h after injection. Blocking was conducted by EGFR saturation with cetuximab 1 day before the experiment and showed significantly reduced uptake ($P < 5.5 \times 10^{-5}$). Data are presented as a mean ± SD; n = 4. Error bars might not be seen because they are smaller than the symbols.

already been reported by Garousi and co-workers.[42] Pretreatment of the mice with cetuximab as blocking agent resulted in a nonblocked-to-blocked tumor ratio of ~12 revealing high specificity of ^{89}Zr-FSC-ZEGFR:2377 binding to EGFR expressing malignant tissue. *Ex vivo* biodistribution of ^{89}Zr-FSC-ZEGFR:2377 and ^{89}Zr-DFO-ZEGFR:2377 labeled at elevated temperature as well as previous published ^{89}Zr-DFO-ZEGFR:2377 labeled at ambient temperature in A431 tumor xenografted nude mice 3 and 24 h after injection is shown in

DOI: 10.1021/acs.molpharmaceut.7b00787
Mol. Pharmaceutics 2018, 15, 175−185

Table 3. Biodistribution of ^{89}Zr-FSC-ZEGFR:2377 and ^{89}Zr-DFO-ZEGFR:2377 in EGFR-Expressing A431 Tumor Xenografted Female BALB/C nu/nu Mice Expressed as Percentage of Injected Dose per Gram Tissue (% ID/g; Mean ± SD; n = 4)[a]

	^{89}Zr-FSC-ZEGFR:2377 (radiolabeling at 85 °C)		^{89}Zr-DFO-ZEGFR:2377 (radiolabeling at 85 °C)		^{89}Zr-DFO-ZEGFR:2377 (radiolabeling at RT)[42]	
organs	3 h	24 h	3 h	24 h	3 h	24 h
blood	1.02 ± 0.29§	0.31 ± 0.08$^{+,\S}$	0.57 ± 0.1$^{*,\#}$	0.25 ± 0.07$^{+,\#}$	2.0 ± 0.38	0.7 ± 0.07^{+}
salivary gland	1.18 ± 0.15	1.08 ± 0.19	0.82 ± 0.11*	0.68 ± 0.18*	0.99 ± 0.25	0.75 ± 0.06§
lung	1.43 ± 0.06	0.88 ± 0.1^{+}	0.83 ± 0.09$^{*,\#}$	0.6 ± 0.09$^{*,\#}$	1.6 ± 0.14	0.98 ± 0.24^{+}
liver	6.71 ± 1.38	5.71 ± 0.94	3.05 ± 0.18$^{*,\#}$	2.37 ± 0.24$^{+,*}$	4.13 ± 0.86§	2.7 ± 0.18$^{+,\S}$
spleen	1.51 ± 0.23	1.38 ± 0.14	0.9 ± 0.13*	0.96 ± 0.13*	0.8 ± 0.12§	0.86 ± 0.19§
colon	1.32 ± 0.09	1.19 ± 0.2	1.12 ± 0.2	0.81 ± 0.12*	1.15 ± 0.32	0.89 ± 0.23
kidney	291.04 ± 19.8	251.54 ± 23.87	283.5 ± 19.01	305.78 ± 63.6	239.05 ± 17.21	232.27 ± 10.56
tumor	8.42 ± 1.53*,§	5.25 ± 0.83$^{+,*,\S}$	5.9 ± 0.48$^{\#}$	3.31 ± 0.57^{+}	4.25 ± 0.63	2.58 ± 0.47^{+}
muscle	0.30 ± 0.04	0.24 ± 0.03^{+}	0.21 ± 0.02$^{*,\#}$	0.18 ± 0.02$^{*,\#}$	0.31 ± 0.02	0.25 ± 0.03^{+}
bone	1.00 ± 0.09	0.99 ± 0.26	0.54 ± 0.23$^{\#}$	1.0 ± 0.31	0.94 ± 0.16	1.77 ± 0.61^{+}

[a]Statistical analysis was performed using the Student's t test with P values indicating significant ($P < 0.05$) difference (+) between 3 and 24 h, (*) between ^{89}Zr-FSC-ZEGFR:2377 (85 °C) and ^{89}Zr-DFO-ZEGFR:2377 (85 °C), (§) between ^{89}Zr-FSC-ZEGFR:2377 (85 °C) and ^{89}Zr-DFO-ZEGFR:2377 (RT) and (#) between ^{89}Zr-DFO-ZEGFR:2377 (85 °C) and ^{89}Zr-DFO-ZEGFR:2377 (RT) at corresponding time points.

Table 4. Tumor-to-Organ Ratios of ^{89}Zr-FSC-ZEGFR:2377 and ^{89}Zr-DFO-ZEGFR:2377 in BALB/C Nude Mice Bearing EGFR-Expressing A431 Tumor Xenograft (Mean ± SD; n = 4)[a]

	^{89}Zr-FSC-ZEGFR:2377 (radiolabeling at 85 °C)		^{89}Zr-DFO-ZEGFR:2377 (radiolabeling at 85 °C)		^{89}Zr-DFO-ZEGFR:2377 (radiolabeling at RT)[42]	
organs	3 h	24 h	3 h	24 h	3 h	24 h
blood	9.0 ± 3.3§	17.5 ± 5.6§	10.6 ± 2.4$^{\#}$	13.7 ± 2.0$^{\#}$	2.2 ± 0.3	3.7 ± 0.6
salivary gland	7.3 ± 2.1§	5.0 ± 1.6	7.3 ± 1.7$^{\#}$	5.1 ± 1.6	4.4 ± 0.8	3.2 ± 0.5
lung	5.9 ± 1.3§	6.0 ± 1.2§	7.2 ± 1.3$^{\#}$	5.7 ± 1.4$^{\#}$	2.7 ± 0.5	2.7 ± 0.4
liver	1.3 ± 0.4	0.9 ± 0.2	1.9 ± 0.3$^{*,\#}$	1.4 ± 0.3$^{*,\#}$	1.1 ± 0.2	1.0 ± 0.1
spleen	5.6 ± 1.2	3.8 ± 0.4	6.6 ± 0.6$^{\#}$	3.5 ± 0.8	5.3 ± 0.4	3.2 ± 1.0
colon	6.4 ± 1.3§	4.5 ± 1.2	5.4 ± 1.1	4.2 ± 1.2	3.9 ± 0.9	3.1 ± 1.2
kidney	0.03 ± 0.006	0.02 ± 0.00	0.02 ± 0.003	0.01 ± 0.00	0.02 ± 0.003	0.01 ± 0.00
muscle	27.9 ± 4.9§	21.9 ± 2.2§	28.4 ± 4.7$^{\#}$	18.6 ± 3.2$^{\#}$	13.6 ± 1.3	10.3 ± 1.2
bone	8.5 ± 1.8§	5.6 ± 1.8§	9.3 ± 2.6$^{\#}$	3.6 ± 1.3$^{\#}$	4.6 ± 0.4	1.6 ± 0.1

[a]Statistical analysis was performed using the Student's t test with P values indicating significant ($P < 0.05$) difference (*) between ^{89}Zr-FSC-ZEGFR:2377 (85 °C) and ^{89}Zr-DFO-ZEGFR:2377 (85 °C), (§) between ^{89}Zr-FSC-ZEGFR:2377 (85 °C) and ^{89}Zr-DFO-ZEGFR:2377 (RT) and (#) between ^{89}Zr-DFO-ZEGFR:2377 (85 °C) and ^{89}Zr-DFO-ZEGFR:2377 (RT) at corresponding time points.

Table 3. Both conjugates labeled at 85 °C showed rapid blood clearance over time, being consistent with the report of Garousi and co-workers, but showed generally lower blood levels than ^{89}Zr-DFO-ZEGFR:2377 labeled at room temperature. Affibody typically excretion via renal pathway and tubular reabsorption resulted in high kidney accumulation and was comparable for ^{89}Zr-FSC-ZEGFR:2377 and ^{89}Zr-DFO-ZEGFR:2377. ^{89}Zr-FSC-ZEGFR:2377 showed no significant decrease of uptake between 3 and 24 h except from lung, muscle and tumor while ^{89}Zr-DFO-ZEGFR:2377 showed differences between liver and tumor. Furthermore, the tumor uptake of ^{89}Zr-FSC-ZEGFR:2377 resulted to be 1.5 fold higher compared to ^{89}Zr-DFO-ZEGFR:2377 labeled at 85 °C and 2 fold higher compared to ^{89}Zr-DFO-ZEGFR:2377 (labeled at room temperature) at both time points. ^{89}Zr-DFO-ZEGFR:2377 showed significantly lower uptake in salivary gland, lung, liver, spleen and muscle compared to ^{89}Zr-FSC-ZEGFR:2377 and lung and muscle compared to ^{89}Zr-DFO-ZEGFR:2377 labeled at room temperature.[42] Corresponding tumor-to-organ ratios as a predictor for imaging contrast are presented in Table 4. Comparing ^{89}Zr-FSC-ZEGFR:2377 and ^{89}Zr-DFO-ZEGFR:2377 the resulting ratios were not significantly different at both time points except from tumor-to-liver ratio which was 1.4 fold higher for ^{89}Zr-DFO-ZEGFR:2377. ^{89}Zr-FSC-ZEGFR:2377 showed increased tumor-to-organ ratios for all tissues except from liver and spleen 3 h p.i and except from liver spleen, salivary gland and colon 24 h p.i compared to ^{89}Zr-DFO-ZEGFR:2377 labeled at ambient temperature. Furthermore, ^{89}Zr-DFO-ZEGFR:2377 labeled at elevated temperature showed increased tumor-to-organ ratios for all organs except from colon 3 h p.i and except from salivary gland, spleen and colon 24 h p.i compared to the data for ^{89}Zr-DFO-ZEGFR:2377 labeled at room temperature.[42]

MicroPET-CT imaging of ^{89}Zr-FSC-ZEGFR:2377 and ^{89}Zr-DFO-ZEGFR:2377 in EGFR-expressing A431 tumor xenografted mice is presented in Figure 6 and is in excellent agreement with the results of the biodistribution studies. EGFR-expressing tumors on the right hind leg were clearly visualized after 3 and 24 h using ^{89}Zr-FSC-ZEGFR:2377 and ^{89}Zr-DFO-ZEGFR:2377 and renal reabsorption was confirmed as the highest accumulation of radioactivity was found in kidneys. Additionally ^{89}Zr-FSC-ZEGFR:2377 showed increased tumor uptake but also liver was visualized whereas ^{89}Zr-DFO-ZEGFR:2377 showed lower liver accumulation. Somewhat inhomogeneous distribution of radioactivity in tumors is in agreement with the results of autoradiography and histochemical staining of tumor sections (Figure S2). Areas of low

DOI: 10.1021/acs.molpharmaceut.7b00787
Mol. Pharmaceutics 2018, 15, 175−185

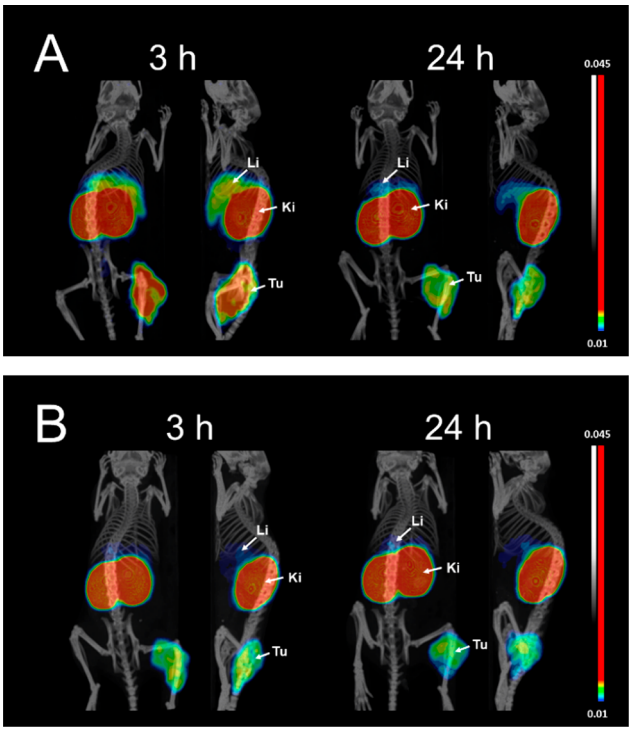

Figure 6. Imaging of EGFR-expression in A431 tumor xenografted BALB/C nu/nu mice using high temperature radiolabeled ^{89}Zr-FSC-ZEGFR:2377 (A) and ^{89}Zr-DFO-ZEGFR:2377 (B) at 3 and 24 h post injection (Li = liver; Ki = kidneys; and Tu = tumor). Coronal/sagittal PET-CT images are shown as maximum intensity projections (MIP) in RGB color scale.

radioactivity uptake were corresponding to necrosis or areas containing more stroma than malignant cells.

DISCUSSION

The results of this study demonstrate that FSC can be site specifically conjugated to ZEGFR:2377 for radiolabeling with zirconium-89 utilizing the same conjugation chemistry as it has been reported for DFO.[42] It is highly noticeable that radiolabeling of both FSC-ZEGFR:2377 and DFO-ZEGFR:2377 at elevated temperature showed significant improvement regarding radiolabeling efficiency, as the radiochemical yield was doubled already after 10 min reaction time (Table 1). Furthermore, high temperature radiolabeling improved the stability of the hexacoordinate ^{89}Zr-ligand complex of FSC-ZEGFR:2377 as EDTA challenging experiments showed a minor release (<3%) of zirconium-89 after 24 h incubation (Table 2). This was not observed for the corresponding DFO conjugate confirming that the cyclic structure of FSC is beneficial for the stability *in vitro* as shown by Zhai and co-workers,[16] which translated in excellent image contrast of ^{89}Zr-labeled RGD-trimers *in vivo*. *Ex vivo* biodistribution studies did not confirm this trend, as ^{89}Zr-FSC-ZEGFR:2377 and ^{89}Zr-DFO-ZEGFR:2377 showed comparable bone uptake without increase over time. Contrary to this for ^{89}Zr-DFO-ZEGFR:2377 labeled at room temperature bone uptake almost doubled after 24 h (Table 3). This is a strong indication that elevated temperature prevents weak off-chelator coordination of zirconium-89 by the protein itself. This is further substantiated by the results of a previous study where FSC was utilized as scaffold for a multivalent integrin targeting RGD ligand radiolabeled with zirconium-89 as small peptides do not offer additional binding pockets for radionuclides. In this study radiolabeling at room temperature was sufficient for stable coordination of zirconium-89 as animal experiments showed generally low bone uptake (~1%) without increasing over time (e.g., 1, 2, and 4 h).[16]

FSC-conjugation did not alter receptor binding or specificity as compared to DFO. Both bioconjugates showed high EGFR affinity (Figure 1) in the picomolar range, being in good agreement with earlier findings.[41,42] Highly specific receptor binding correlating with the level of EGFR-expression for ^{89}Zr-FSC-ZEGFR:2377 is shown in Figure 2. Internalization on A431 cells (Figure 3) was slow and somewhat lower compared to previous reports on ^{89}Zr-DFO-ZEGFR:2377,[42] ^{99m}Tc-ZEGFR:2377,[41] and ^{111}In-DOTA-ZEGFR:2377.[43] *In vivo* specificity results of ^{89}Zr-FSC-ZEGFR:2377 were similar to the data from Garousi and co-workers[42] except from liver uptake. ^{89}Zr-FSC-ZEGFR:2377 liver uptake was 2-fold higher compared to ^{89}Zr-DFO-ZEGFR:2377 and showed no significant reduction after EGFR presaturation with cetuximab, indicating that this uptake is compound not receptor related. The extraordinary high radioactivity accumulation in kidney tissue is a common feature of radiometal labeled affibody molecules due to prevalent renal elimination followed by tubular reabsorption. The exact molecular mechanism is still not fully understood, but it is clear that the uptake is not megalin-dependent and cannot be prevented by pre- or coinjection of cationic amino acids or Gelofusine.[48] This might be limiting toward affibody-mediated radionuclide therapy but is tolerable in case of diagnostic imaging, an equally high renal uptake of anti-HER2 affibody molecules did not prevent clinical imaging of metastases in lumbar area.[49,50] ^{89}Zr-FSC-ZEGFR:2377 showed slower blood clearance in comparison to ^{89}Zr-DFO-ZEGFR:2377 resulting in slightly increased uptake in normal tissue but also significantly higher tumor uptake especially 3 h p.i. indicating higher bioavailability[51] of ^{89}Zr-FSC-ZEGFR:2377. Corresponding tumor-to-organ ratios (Table 4) were not significantly different except from liver indicating that ^{89}Zr-FSC-ZEGFR:2377 is equivalent to ^{89}Zr-DFO-ZEGFR:2377 for imaging of EGFR-expression *in vivo*. This was confirmed by small animal PET-CT in A431 tumor xenografted mice (Figure 5). Lower tumor-to-liver ratio of ^{89}Zr-FSC-ZEGFR:2377 might be disadvantageous toward sensitivity against EGFR-expressing liver metastases but might be compensated by the higher tumor uptake. The most striking difference was observed between ^{89}Zr-ZEGFR:2377 conjugates labeled at elevated temperature and ^{89}Zr-DFO-ZEGFR:2377 labeled at room temperature.[42] Tumor-to-organ ratios were generally significantly higher allowing to detect EGFR-expression with higher contrast and therefore improved sensitivity. This should be taken into account for radiolabeling of biomolecules with zirconium-89. In case of heat sensitive molecules, pre-radiolabeling approaches, where radiolabeling is carried out prior to conjugation to the biomolecule, may lead to improved targeting. In comparison to other EGFR-affibody tracers evaluated in the same mouse model (e.g., Al^{18}F-NOTA-ZEGFR:1907[44], ^{18}F-CBT-ZEGFR:1907,[44] and ^{18}F-FBEM-Cys-ZEGFR:1907[52]) both ^{89}Zr-DFO- and ^{89}Zr-FSC-ZEGFR:2377 showed ~5-fold higher tumor-to-blood ratio. Additionally ^{89}Zr-panitumumab[35] and ^{89}Zr-cetuximab[53] in A431 xenografted mice showed ~5-fold lower tumor-to-blood ratios after 120 and 96 h, respectively. This indicates that both ^{89}Zr-FSC-ZEGFR:2377 as well as ^{89}Zr-DFO-ZEGFR:2377 are very good radiotracers for imaging of EGFR-related diseases already

DOI: 10.1021/acs.molpharmaceut.7b00787
Mol. Pharmaceutics 2018, 15, 175−185

3 h after administration, but imaging at 24 h would increase imaging contrast further.

It has to be noted that efficient and more stable radiolabeling at elevated temperature might be a limitation for the use of FSC for radiolabeling of heat sensitive biomolecules, e.g. monoclonal antibodies. Such targeting vectors would require alternative approaches for stable radiolabeling with zirconium-89. A number of novel chelators are under development for this purpose, as it is described in the recent review by Heskamp and co-workers.[54] Particularly, such chelators as DFO*, DFO-Sq, and HOPO enable radiolabeling at lower temperature and seem to be a good alternative to DFO and FSC for this purpose. However, so far it has not been shown that they are also superior to DFO when labeled at higher temperatures.

CONCLUSION

The results of this study showed that FSC is a suitable alternative to DFO as chelating scaffold for EGFR-targeting affibody molecules radiolabeled with zirconium-89. Furthermore, our findings indicate that radiolabeling at elevated temperature increases complex stability and tumor-to-organ ratios resulting in considerably improved imaging properties of ^{89}Zr-DFO-bioconjugates.

ASSOCIATED CONTENT

Supporting Information

The Supporting Information is available free of charge on the ACS Publications website at DOI: 10.1021/acs.molpharmaceut.7b00787.

Representative ESI-MS chromatogram of FSC-ZEGFR:2377 and representative autoradiography and hematoxylin and eosin staining of A431 tumor section obtained at 24 h after injection of ^{89}Zr-FSC-ZEGFR:2377 (PDF)

AUTHOR INFORMATION

Corresponding Author

*E-mail: Clemens.Decristoforo@i-med.ac.at; Tel: +4351250480951; Fax:+435125046780951.

ORCID

Dominik Summer: 0000-0002-1352-5370

Clemens Decristoforo: 0000-0003-0566-4036

Author Contributions

⊥D.S., J.G., and M.O. contributed equally to this work.

Notes

The authors declare the following competing financial interest(s): Vladimir Tolmachev, John Loefblom, and Anna Orlova are the members of the scientific advisory board of Affibody AB. Other authors declare no potentially competing interests.

ACKNOWLEDGMENTS

The authors gratefully acknowledge Herbert Lindner and Leopold Kremser, Innsbruck Medical University, Biocenter/Division of Clinical Biochemistry for performing ESI-MS analysis. This study was financially supported by the Austrian Science Foundation (FWF) grant P 25899-B23, the Swedish Cancer Society (Cancerfonden) grant CAN 2014/474 and CAN2015/350, and the Swedish Research Council (Vetenskapsrådet), grants VR 2015-02509 and VR 2015-02353. The molecular imaging work in this publication was performed at SciLifeLab Pilot Facility for Preclinical PET-MRI, a Swedish nationally available imaging platform at Uppsala University, Sweden, financed by Knut and Alice Wallenberg Foundation (PET/CT).

ABBREVIATIONS USED

FSC, fusarinine C; DFO, desferrioxamine B; EGF(R), epidermal growth factor (receptor); PET, positron emission tomography; mAbs, monoclonal antibodies; ZEGFR:2377, EGFR targeting affibody molecule; RP-HPLC, reversed-phase high-performance liquid chromatography; ITLC, instant thin layer chromatography; RT, room temperature; PBS, phosphate buffered saline; HEPES, 4-(2-hydroxyethyl)-1-piperazineethanesulfonic acid; EDTA, thylenediaminetetraacetic acid

REFERENCES

(1) Wadas, T. J.; Wong, E. H.; Weisman, G. R.; Anderson, C. J. Coordinating Radiometals of Copper, Gallium, Indium, Yttrium, and Zirconium for PET and SPECT Imaging of Disease. *Chem. Rev.* **2010**, *110* (5), 2858−2902.

(2) Mcinnes, L. E.; Rudd, S. E.; Donnelly, P. S. Copper, Gallium and Zirconium Positron Emission Tomography Imaging Agents: The Importance of Metal Ion Speciation. *Coord. Chem. Rev.* **2017**, *352*, 499.

(3) Pandya, D. N.; Bhatt, N.; Yuan, H.; Day, C. S.; Ehrmann, B. M.; Wright, M.; Bierbach, U.; Wadas, T. J. Zirconium Tetraazamacrocycle Complexes Display Extraordinary Stability and Provide a New Strategy for Zirconium-89-Based Radiopharmaceutical Development. *Chem. Sci.* **2017**, *8*, 2309−2314.

(4) Bhatt, N. B.; Pandya, D. N.; Xu, J.; Tatum, D.; Magda, D.; Wadas, T. J. Evaluation of Macrocyclic Hydroxyisophthalamide Ligands as Chelators for Zirconium-89. *PLoS One* **2017**, *12*, e0178767.

(5) Rousseau, J.; Zhang, Z.; Dias, G. M.; Zhang, C.; Colpo, N.; Bénard, F.; Lin, K. S. Design, Synthesis and Evaluation of Novel Bifunctional Tetrahydroxamate Chelators for PET Imaging of ^{89}Zr-Labeled Antibodies. *Bioorg. Med. Chem. Lett.* **2017**, *27* (4), 708−712.

(6) Deri, M. A.; Ponnala, S.; Zeglis, B. M.; Pohl, G.; Dannenberg, J. J.; Lewis, J. S.; Francesconi, L. C. Alternative Chelator for ^{89}Zr Radiopharaceuticals: Radiolabeling and Evaluatioin of 3,4,3-(LI-1,2-HOPO). *J. Med. Chem.* **2014**, *57*, 4849−4860.

(7) Guérard, F.; Lee, Y.-S.; Brechbiel, M. W. Rational Design, Synthesis and Evaluation of Tetrahydroxamic Acid Chelators for Stable Complexation of ZrIV. *Chem. - Eur. J.* **2014**, *20* (19), 5584−5591.

(8) Patra, M.; Bauman, A.; Mari, C.; Fischer, C. A.; Blacque, O.; Häussinger, D.; Gasser, G.; Mindt, T. L. An Octadentate Bifunctional Chelating Agent for the Development of Stable Zirconium-89 Based Molecular Imaging Probes. *Chem. Commun.* **2014**, *50* (78), 11523−11525.

(9) Ma, M. T.; Meszaros, L. K.; Paterson, B. M.; Berry, D. J.; Cooper, M. S.; Ma, Y.; Hider, R. C.; Blower, P. J. Tripodal Tris-(hydroxypyridinone) Ligands for Immunoconjugate PET Imaging with ^{89}Zr(4+): Comparison with Desferrioxamine-B. *Dalton Trans.* **2015**, *44* (11), 4884−4900.

(10) Jansen, M. H.; Veldhuijzen van Zanten, S. E. M.; van Vuurden, D. G.; Huisman, M. C.; Vugts, D. J.; Hoekstra, O. S.; van Dongen, G. A.; Kaspers, G.-J. L. Molecular Drug Imaging: ^{89}Zr-Bevacizumab PET in Children with Diffuse Intrinsic Pontine Glioma. *J. Nucl. Med.* **2017**, *58* (5), 711−716.

(11) Ulaner, G. A.; Hyman, D. M.; Ross, D. S.; Corben, A.; Chandarlapaty, S.; Goldfarb, S.; McArthur, H.; Erinjeri, J. P.; Solomon, S. B.; Kolb, H.; Lyashchenko, S. K.; Lewis, J. S.; Carrasquillo, J. A. Detection of HER2-Positive Metastases in Patients with HER2-Negative Primary Breast Cancer Using ^{89}Zr-Trastuzumab PET/CT. *J. Nucl. Med.* **2016**, *57* (10), 1523−1528.

(12) Menke van der Houven van Oordt, C. W.; Gootjes, E. C.; Huisman, M. C.; Vugts, D. J.; Roth, C.; Luik, A. M.; Mulder, E. R.; Schuit, R. C.; Boellaard, R.; Hoekstra, O. S.; van Dongen, G. A. M. S.;

DOI: 10.1021/acs.molpharmaceut.7b00787
Mol. Pharmaceutics 2018, 15, 175−185

Verheul, H. M. W. ^{89}Zr-Cetuximab PET Imaging in Patients with Advanced Colorectal Cancer. *Oncotarget* **2015**, *6* (30), 30384.
(13) Holland, J. P.; Divilov, V.; Bander, N. H.; Smith-Jones, P. M.; Larson, S. M.; Lewis, J. S. 89Zr-DFO-J591 for immunoPET Imaging of Prostate-Specific Membrane Antigen (PSMA) Expression in Vivo. *J. Nucl. Med.* **2010**, *51* (8), 1293−1300.
(14) Chang, A. J.; DeSilva, R.; Jain, S.; Lears, K.; Rogers, B.; Lapi, S. ^{89}Zr-Radiolabeled Trastuzumab Imaging in Orthotopic and Metastatic Breast Tumors. *Pharmaceuticals* **2012**, *5* (1), 79−93.
(15) Schrettl, M.; Bignell, E.; Kragl, C.; Sabiha, Y.; Loss, O.; Eisendle, M.; Wallner, A.; Arst, H. N.; Haynes, K.; Haas, H. Distinct Roles for Intra- and Extracellular Siderophores during Aspergillus Fumigatus Infection. *PLoS Pathog.* **2007**, *3* (9), 1195−1207.
(16) Zhai, C.; Summer, D.; Rangger, C.; Franssen, G. M.; Laverman, P.; Haas, H.; Petrik, M.; Haubner, R.; Decristoforo, C. Novel Bifunctional Cyclic Chelator for ^{89}Zr Labeling-Radiolabeling and Targeting Properties of RGD Conjugates. *Mol. Pharmaceutics* **2015**, *12* (6), 2142−2150.
(17) Stern, L. A.; Case, B. A.; Hackel, B. J. Alternative Non-Antibody Protein Scaffolds for Molecular Imaging of Cancer. *Curr. Opin. Chem. Eng.* **2013**, *2* (4), 425.
(18) Simeon, R.; Chen, Z. In Vitro-Engineered Non-Antibody Protein Therapeutics. *Protein Cell* **2017**, 1−12.
(19) Orlova, A.; Nilsson, F. Y.; Wikman, M.; Widström, C.; Ståhl, S.; Carlsson, J.; Tolmachev, V. Comparative in Vivo Evaluation of Technetium and Iodine Labels on an Anti-HER2 Affibody for Single-Photon Imaging of HER2 Expression in Tumors. *J. Nucl. Med.* **2006**, *47* (3), 512−519.
(20) Ekblad, T.; Orlova, A.; Feldwisch, J.; Wennborg, A.; Karlström, A. E.; Tolmachev, V. Positioning of ^{99m}Tc-Chelators Influences Radiolabeling, Stability and Biodistribution of Affibody Molecules. *Bioorg. Med. Chem. Lett.* **2009**, *19* (14), 3912−3914.
(21) Lindberg, H.; Hofström, C.; Altai, M.; Honorvar, H.; Wållberg, H.; Orlova, A.; Ståhl, S.; Gräslund, T.; Tolmachev, V. Evaluation of a HER2-Targeting Affibody Molecule Combining an N-Terminal HEHEHE-Tag with a GGGC Chelator for ^{99m}Tc-Labelling at the C Terminus. *Tumor Biol.* **2012**, *33* (3), 641−651.
(22) Tolmachev, V.; Yim, C.-B.; Rajander, J.; Perols, A.; Karlstrom, A. E.; Haaparanta-Solin, M.; Gronroos, T. J.; Solin, O.; Orlova, A. Comparative Evaluation of Anti-HER2 Affibody Molecules Labeled with ^{64}Cu Using NOTA and NODAGA. *Contrast Media Mol. Imaging* **2017**, *2017*, 8565802.
(23) Terwisscha van Scheltinga, A. G. T.; Lub-de Hooge, M. N.; Hinner, M. J.; Verheijen, R. B.; Allersdorfer, A.; Hulsmeyer, M.; Nagengast, W. B.; Schroder, C. P.; Kosterink, J. G. W.; de Vries, E. G. E.; Audoly, L.; Olwill, S. A. In Vivo Visualization of MET Tumor Expression and Anticalin Biodistribution with the MET-Specific Anticalin ^{89}Zr-PRS-110 PET Tracer. *J. Nucl. Med.* **2014**, *55* (4), 665−671.
(24) Tolmachev, V.; Rosik, D.; Wållberg, H.; Sjöberg, A.; Sandström, M.; Hansson, M.; Wennborg, A.; Orlova, A. Imaging of EGFR Expression in Murine Xenografts Using Site-Specifically Labelled Anti-EGFR In-DOTA-Z EGFR: 2377 Affibody Molecule: Aspect of the Injected Tracer Amount. *Eur. J. Nucl. Med. Mol. Imaging* **2010**, *37*, 613−622.
(25) Wee, P.; Wang, Z. Epidermal Growth Factor Receptor Cell Proliferation Signaling Pathways. *Cancers* **2017**, *9* (5), 52.
(26) Bentzen, S. M.; Atasoy, B. M.; Daley, F. M.; Dische, S.; Richman, P. I.; Saunders, M. I.; Trott, K. R.; Wilson, G. D. Epidermal Growth Factor Receptor Expression in Pretreatment Biopsies From Head and Neck Squamous Cell Carcinoma As a Predictive Factor for a Benefit From Accelerated Radiation Therapy in a Randomized Controlled Trial. *J. Clin. Oncol.* **2005**, *23* (24), 5560−5567.
(27) Ang, K. K.; Berkey, B. A.; Tu, X.; Zhang, H.; Katz, R.; Hammond, E. H.; Fu, K. K. Impact of Epidermal Growth Factor Receptor Expression on Survival and Pattern of Relapse in Patients with Advanced Head and Neck Carcinoma 1. *Cancer Res.* **2002**, *62*, 7350−7356.
(28) Pirker, R.; Pereira, J. R.; von Pawel, J.; Krzakowski, M.; Ramlau, R.; Park, K.; Marinis, F.; De Eberhardt, W. E. E.; Paulo, S.; et al. EGFR Expression as a Predictor of Survival for First-Line Chemotherapy plus Cetuximab in Patients with Advanced Non-Small-Cell Lung Cancer: Analysis of Data from the Phase 3. *Lancet Oncol.* **2012**, *13* (1), 33−42.
(29) Hirsch, F. R.; Varella-Garcia, M.; Bunn, P. A., Jr; Franklin, W. A.; Dziadziuszko, R.; Thatcher, N.; Chang, A.; Parikh, P.; Pereira, J. R.; Ciuleanu, T.; von Pawel, J.; Watkins, C.; Flannery, A.; Ellison, G.; Donald, E.; Knight, L.; Parums, D.; Botwood, N.; Holloway, B. Molecular Predictors of Outcome With Gefitinib in a Phase III Placebo-Controlled Study in Advanced Non − Small- Cell Lung Cancer. *J. Clin. Oncol.* **2006**, *24* (31), 5034−5042.
(30) Cappuzzo, F.; Hirsch, F. R.; Rossi, E.; Bartolini, S.; Ceresoli, G. L.; Bemis, L.; Haney, J.; Witta, S.; Danenberg, K.; Ludovini, V.; Magrini, E.; Gregorc, V.; Sidoni, A.; Tonato, M.; Franklin, W. A.; Crino, L.; Bunn, P. A.; Varella-Garcia, M.; Domenichini, I.; Doglioni, C. Epidermal Growth Factor Receptor Gene and Protein and Ge Fi Tinib Sensitivity in Non-Small-Cell Lung Cancer. *J. Natl. Cancer Inst.* **2005**, *97* (9), 643−655.
(31) Roskoski, R. J. The ErbB/HER Family of Protein-Tyrosine Kinases and Cancer. *Pharmacol. Res.* **2014**, *79*, 34−74.
(32) Chung, K. Y.; Shia, J.; Kemeny, N. E.; Shah, M.; Schwartz, G. K.; Tse, A.; Hamilton, A.; Pan, D.; Schrag, D.; Schwartz, L.; Klimstra, D. S.; Fridman, D.; Kelsen, D. P.; Saltz, L. B. Cetuximab Shows Activity in Colorectal Cancer Patients with Tumors That Do Not Express the Epidermal Growth Factor Receptor by Immunohistochemistry. *J. Clin. Oncol.* **2005**, *23* (9), 1803−1810.
(33) Divgi, C. R.; Welt, S.; Kris, M.; Real, F. X.; Yeh, S. D.; Gralla, R.; Merchant, B.; Schweighart, S.; Unger, M.; Larson, S. M.; Mendelsohn, J. Phase I and Imaging Trial of Indium 111-Labeled Anti-Epidermal Growth Factor Receptor Monoclonal Antibody 225 in Patients with Squamous Cell Lung Carcinoma. *J. Natl. Cancer Inst.* **1991**, *83* (2), 97−104.
(34) Velikyan, I.; Sundberg, Å. L.; Lindhe, Ö.; Höglund, A. U.; Eriksson, O.; Werner, E.; Carlsoon, J.; Bergström, M.; Langström, B.; Tolmachev, V. Preparation and Evaluation of ^{68}Ga-DOTA-hEGF for Visualization of EGFR Expression in Malignant Tumors. *J. Nucl. Med.* **2005**, *46* (13), 1881−1888.
(35) Chang, A. J.; De Silva, R. A.; Lapi, S. E. Development and Characterization of 89 Zr-Labeled Panitumumab for Immuno−Positron Emission Tomographic Imaging of the Epidermal Growth Factor Receptor. *Mol. Imaging* **2013**, *12* (1), 17−27.
(36) Perk, L. R.; Visser, G. W.; Vosjan, M. J.; Stigter-van, W. M.; Tijink, B. M.; Leemans, C. R.; van Dongen, G. A. ^{89}Zr as a PET Surrogate Radioisotope for Scouting Biodistribution of the Therapeutic Radiometals ^{90}Y and ^{177}Lu in Tumor-Bearing Nude Mice After Coupling to the Internalizing Antibody Cetuximab. *J. Nucl. Med.* **2005**, *46* (11), 1898−1906.
(37) van Loon, J.; Even, A. J. G.; Aerts, H. J. W. L.; Öllers, M.; Hoebers, F.; van Elmpt, W.; Dubois, L.; Dingemans, A.-M. C.; Lalisang, R. I.; Kempers, P.; Brans, B.; Winnepenninckx, V.; Speel, E.-J.; Thunnissen, E.; Smits, K. M.; Boellaard, R.; Vugts, D. J.; De Ruysscher, D.; Lambin, P. PET Imaging of Zirconium-89 Labelled Cetuximab: A Phase I Trial in Patients with Head and Neck and Lung Cancer. *Radiother. Oncol.* **2017**, *122* (2), 267−273.
(38) Löfblom, J.; Feldwisch, J.; Tolmachev, V.; Carlsson, J.; Ståhl, S.; Frejd, F. Y. Affibody Molecules: Engineered Proteins for Therapeutic, Diagnostic and Biotechnological Applications. *FEBS Lett.* **2010**, *584* (12), 2670−2680.
(39) Friedman, M.; Orlova, A.; Johansson, E.; Eriksson, T. L. J.; Höidén-Guthenberg, I.; Tolmachev, V.; Nilsson, F. Y.; Ståhl, S. Directed Evolution to Low Nanomolar Affinity of a Tumor-Targeting Epidermal Growth Factor Receptor-Binding Affibody Molecule. *J. Mol. Biol.* **2008**, *376* (5), 1388−1402.
(40) Tolmachev, V.; Friedman, M.; Sandstrom, M.; Eriksson, T. L. J.; Rosik, D.; Hodik, M.; Stahl, S.; Frejd, F. Y.; Orlova, A. Affibody Molecules for Epidermal Growth Factor Receptor Targeting In Vivo: Aspects of Dimerization and Labeling Chemistry. *J. Nucl. Med.* **2009**, *50* (2), 274−283.

DOI: 10.1021/acs.molpharmaceut.7b00787
Mol. Pharmaceutics 2018, 15, 175−185

(41) Andersson, K.; Oroujeni, M.; Garousi, J.; Mitran, B.; Ståhl, S.; Orlova, A.; Löfblom, J.; Tolmachev, V. Feasibility of Imaging of Epidermal Growth Factor Receptor Expression with ZEGFR:2377 Affibody Molecule Labeled with ^{99m}Tc Using a Peptide-Based Cysteine-Containing Chelator. *Int. J. Oncol.* **2016**, DOI: 10.3892/ijo.2016.3721.
(42) Garousi, J.; Andersson, K. G.; Mitran, B.; Pichl, M. L.; Stahl, S.; Orlova, A.; Löfblom, J.; Tolmachev, V. PET Imaging of Epidermal Growth Factor Receptor Expression in Tumours Using ^{89}Zr-Labelled ZEGFR:2377 Affibody Molecules. *Int. J. Oncol.* **2016**, *48* (4), 1325−1332.
(43) Tolmachev, V.; Rosik, D.; Wållberg, H.; Sjöberg, A.; Sandström, M.; Hansson, M.; Wennborg, A.; Orlova, A. Imaging of EGFR Expression in Murine Xenografts Using Site-Specifically Labelled Anti-EGFR ^{111}In-DOTA-ZEGFR:2377 Affibody Molecule: Aspect of the Injected Tracer Amount. *Eur. J. Nucl. Med. Mol. Imaging* **2010**, *37* (3), 613−622.
(44) Su, X.; Cheng, K.; Jeon, J.; Shen, B.; Venturin, G. T.; Hu, X.; Rao, J.; Chin, F. T.; Wu, H.; Cheng, Z. Comparison of Two Site-Specifically ^{18}F-Labeled Affibodies for PET Imaging of EGFR Positive Tumors. *Mol. Pharmaceutics* **2014**, *11*, 3947−3956.
(45) Summer, D.; Grossrubatscher, L.; Petrik, M.; Michalcikova, T.; Novy, Z.; Rangger, C.; Klingler, M.; Haas, H.; Kaeopookum, P.; von Guggenberg, E.; Haubner, R.; Decristoforo, C. Developing Targeted Hybrid Imaging Probes by Chelator Scaffolding. *Bioconjugate Chem.* **2017**, *28*, 1722.
(46) Vosjan, M. J. W. D.; Perk, L. R.; Visser, G. W. M.; Budde, M.; Jurek, P.; Kiefer, G. E.; van Dongen, G. A. M. S. Conjugation and Radiolabeling of Monoclonal Antibodies with Zirconium-89 for PET Imaging Using the Bifunctional Chelate P-Isothiocyanatobenzyl-Desferrioxamine. *Nat. Protoc.* **2010**, *5* (4), 739−743.
(47) Barta, P.; Malmberg, J.; Melicharova, L.; Strandgård, J.; Orlova, A.; Tolmachev, V.; Laznicek, M.; Andersson, K. Protein Interactions with HER-Family Receptors Can Have Different Characteristics Depending on the Hosting Cell Line. *Int. J. Oncol.* **2012**, *40* (5), 1677−1682.
(48) Vegt, E.; de Jong, M.; Wetzels, J. F. M.; Masereeuw, R.; Melis, M.; Oyen, W. J. G.; Gotthardt, M.; Boerman, O. C. Renal Toxicity of Radiolabeled Peptides and Antibody Fragments: Mechanisms, Impact on Radionuclide Therapy, and Strategies for Prevention. *J. Nucl. Med.* **2010**, *51* (7), 1049−1058.
(49) Sörensen, J.; Sandberg, D.; Sandström, M.; Wennborg, A.; Feldwisch, J.; Tolmachev, V.; Aström, G.; Lubberink, M.; Garske-Román, U.; Carlsson, J.; Lindman, H. First-in-HumanMolecular Imaging of HER2 Expression in Breast Cancer Metastases Using the 111In-ABY-025 Affibody Molecule Jens. *J. Nucl. Med.* **2014**, *55* (5), 730−736.
(50) Sörensen, J.; Velikyan, I.; Sandberg, D.; Wennborg, A.; Feldwisch, J.; Orlova, A.; Sandström, M.; Lubberink, M.; Olofsson, H.; Carlsson, J.; Lindman, H.; Tolmachev, V. Measuring HER2-Receptor Expression In Metastatic Breast Cancer Using [^{68}Ga]ABY-025 Affibody PET/CT. *Theranostics* **2016**, *6* (2), 262−271.
(51) Rosik, D.; Orlova, A.; Malmberg, J.; Altai, M.; Varasteh, Z.; Sandström, M.; Karlström, A. E.; Tolmachev, V. Direct Comparison of ^{111}In-Labelled Two-Helix and Three-Helix Affibody Molecules for in Vivo Molecular Imaging. *Eur. J. Nucl. Med. Mol. Imaging* **2012**, *39* (4), 693−702.
(52) Miao, Z.; Ren, G.; Liu, H.; Qi, S.; Wu, S.; Cheng, Z. PET of EGFR Expression with an ^{18}F-Labeled Affibody Molecule. *J. Nucl. Med.* **2012**, *53* (7), 1110−1118.
(53) Aerts, H. J. W. L.; Dubois, L.; Perk, L.; Vermaelen, P.; van Dongen, G. A. M. S.; Wouters, B. G.; Lambin, P. Disparity Between In Vivo EGFR Expression and ^{89}Zr-Labeled Cetuximab Uptake Assessed with PET. *J. Nucl. Med.* **2008**, *50* (1), 123−131.
(54) Heskamp, S.; Raavé, R.; Boerman, O. C.; Rijpkema, M.; Goncalves, V.; Denat, F. ^{89}Zr-immunoPET in Oncology: State of the Art ^{89} Zr-Radiochemistry. *Bioconjugate Chem.* **2017**, *28*, 2211.

DOI: 10.1021/acs.molpharmaceut.7b00787
Mol. Pharmaceutics 2018, 15, 175−185